Adiabatic effects on radiation belt electrons at low altitude

Weichao Tu[1,2] and Xinlin Li[1,2]

[1]   The storm-time adiabatic effects of radiation belt electrons mirroring at low altitude are not analogous to those of equatorially mirroring electrons. During the main phase of a geomagnetic storm the adiabatic effects on low-altitude electrons include the expansion of the drift shell, the rise of the mirror point in altitude that is unique for electrons mirroring off-equator, and the shift in the energy spectrum. Calculations of the adiabatic flux change at low altitudes using a modified dipole model demonstrate that the storm-time adiabatic effects on electron flux are both altitude- and storm-dependent. The rise of the electron mirror points can lead to a null flux region at the low altitudes. A satellite in the null flux region sees zero flux during the storm time due solely to adiabatic effects, which can persist when the nonadiabatic pitch angle diffusion is very slow. A low-altitude satellite above the null flux region will see a fractional flux drop due to the adiabatic effects. For example, for the March 2008 geomagnetic storm with minimum Dst of -72 nT, there would be a factor of 2.4–2.8 decrease in the flux of relativistic electrons mirroring at 700 km and $L^* = 4.5$, compared to a decrease of a factor of ~15 for equatorially mirroring electrons due to adiabatic effects. We propose that the resulting adiabatic change in the electron pitch angle distribution can cause increased electron precipitation without changing the pitch angle diffusion rate by exciting higher-order eigenmodes of the bounce-averaged pitch angle diffusion. This work is the first quantitative analysis combining both observation and modeling for the adiabatic effects on the variation of outer radiation belt electrons at low altitude.

1.   Introduction

[2]   Outer radiation belt MeV electron fluxes vary greatly during geomagnetic storms [e.g., *Baker and Kanekal*, 2008; *Tu et al.*, 2009]. They are observed to decrease during storm main phases and increase in storm recovery phases [e.g., *Reeves et al.*, 2003; *Tu et al.*, 2010]. The causes of these variations can be classified into adiabatic and nonadiabatic processes [e.g., *Li and Temerin*, 2001; *Friedel et al.*, 2002; *Millan and Thorne*, 2007; and references therein]. Nonadiabatic processes cause irreversible electron variations by breaking at least one of the three adiabatic invariants [e.g., *Li et al.*, 1997; *Tu et al.*, 2009]; adiabatic processes cause reversible variations [*Li et al.*, 1997; *Kim and Chan*, 1997; *Selesnick and Kanekal*, 2009]. The classification is quite clear, but since the observed changes are a mixed result of both processes, distinguishing between them by looking at the data alone is difficult. This warrants a quantitative analysis of pure adiabatic variations, which will help to determine the real (or nonadiabatic) losses in the radiation belt system.

[3]   The topic of adiabatic variations of radiation belt electrons is not new [e.g., *McIlwain*, 1966, 1996]. Based on the resemblance of the temporal profile of energetic electron fluxes to the *Dst* profile, *Li et al.* [1997] introduced the term "*Dst* effect" to describe the adiabatic effects on energetic electrons due to changes in the magnetic field from the storm time ring current. *Kim and Chan* [1997] showed that adiabatic effects cause flux decreases of more than an order of magnitude for 1 MeV and 2 MeV electrons mirroring at the equator when *Dst* reaches -100 nT. Here, however, we focus on (smaller pitch angle) electrons mirroring at low altitudes.

[4]   Electron intensity variations measured by SAMPEX, a satellite in a low-altitude, polar orbit ($\sim$600 km, 82°) [*Baker et al.*, 1993], also seem to correlate well with *Dst*, as shown in Figure 1. The top three panels in Figure 1a show the daily averaged electron count rates (color-coded) observed by SAMPEX/PET from three different counters (P1, ELO and EHI) [*Cook et al.*, 1993]. In each panel, the *x* axis is time during the March 2008 storm and the *y* axis is L (the radial distance of the magnetic field line in the equatorial plane under the dipole field approximation). The electron count rate drops significantly during the storm main phase and recovers as *Dst* recovers. Figure 1a leads to our first question: are these storm-time variations adiabatic responses to geomagnetic field variations? We expand the daily averaged data in more detail to look at variations at fixed L in Figure 1b. The first panel contains data from a day before the storm, the second
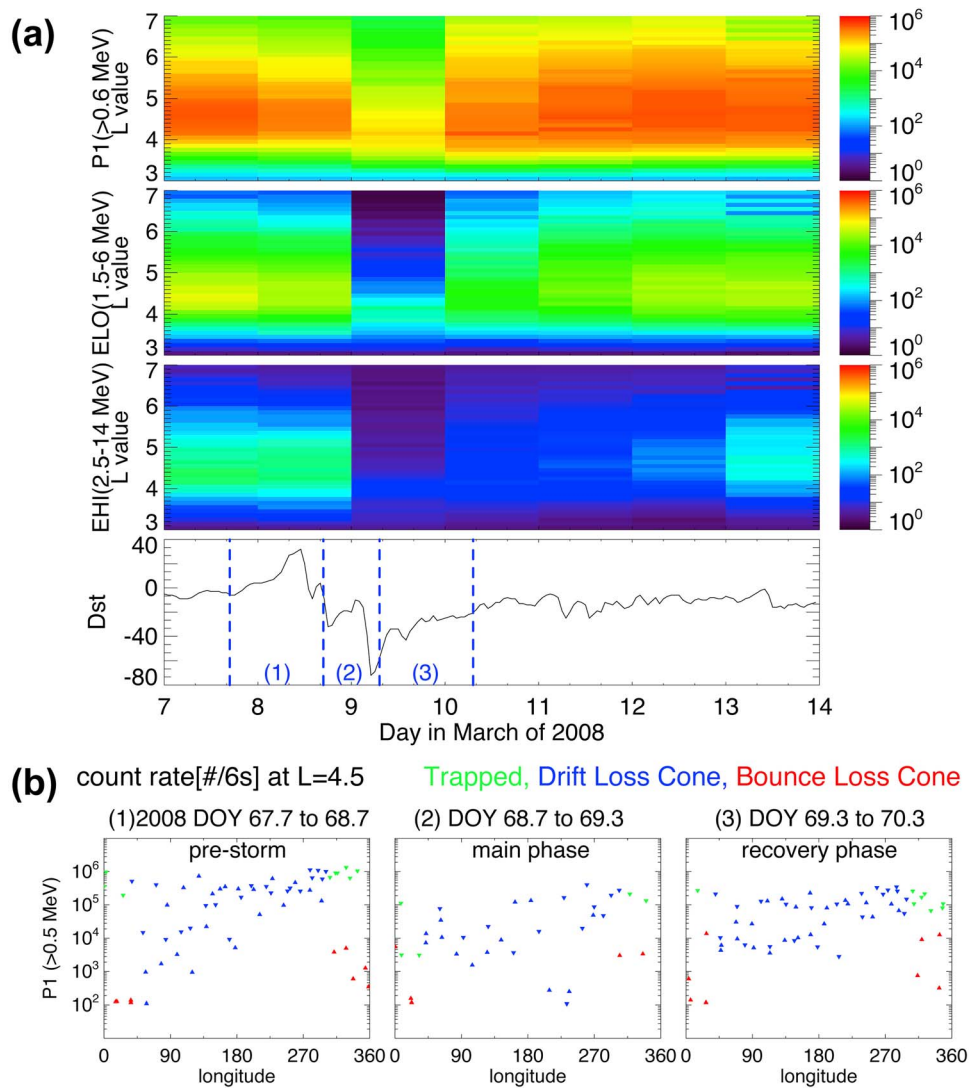
Figure 1. (a) The top three panels show the electron count rate during the March 2008 storm detected by three SAMPEX/PET counters: P1, ELO, and EHI, respectively. The count rates, in units of #/6 s, are daily averaged (x axis), color-coded in logarithm (color bar on the right), and sorted in L (L bin: 0.1 y axis). The fourth panel shows the *Dst* data during this storm. (b) The electron count rate data at L = 4.5 from the P1 counter during (1) a quiet prestorm interval, (2) storm main phase, and (3) early recovery phase of the March 2008 storm. The three intervals are marked in the *Dst* profile above.

panel shows half a day during the storm main phase and the third panel is in the early recovery phase. Within each panel, the data points are organized in geomagnetic longitude to distinguish them as trapped, drift loss cone, and bounce loss cone electrons. For a more detailed description of these data, refer to Figure 2 in the work of *Tu et al.* [2010]. Figure 1b suggests that the trapped electron count rates (green points) at L = 4.5 dropped by almost an order of magnitude during the storm main phase. The second question we would like to address is: quantitatively, how much of the main phase intensity drop is due to the adiabatic effects?

2. Adiabatic Effects at Low Altitudes

[5] The three adiabatic invariants are $\mu = p_\perp^2/2m_0 B$ (the first invariant), $J = \oint p_\parallel ds$ (the second invariant, more often we use the derived quantity $K = J/2\sqrt{2m_0\mu}$), and $\Phi = \oint \vec{B} d\vec{A}$

(the third invariant, on which Roederer L is defined as $L^* = 2\pi M/(\Phi R_E)$, where M is Earth's magnetic moment) [*Roederer*, 1970]. Here we are interested in fully adiabatic processes in which all three adiabatic invariants are conserved.

[6] There are three adiabatic effects on electrons mirroring at low altitude, each related to the conservation of one adiabatic invariant [*Selesnick*, 2006]. First, as a storm develops, the ring current builds up and decreases the magnetic field in the inner magnetosphere. To conserve the third adiabatic invariant drift shells expand radially. As illustrated by Figure 2a, the projection of the drift shell at $L^* = 4.5$ expands from the black field line at *Dst* = 0 nT to the red field line at *Dst* = −72 nT (minimum *Dst* of the March 2008 storm). Second, due to the stretching of the field line, to conserve the second adiabatic invariant K, the electron mirror point rises in altitude (from point P_1 to P_2). The field lines and mirror point locations in Figure 2 are calculated using the modified dipole
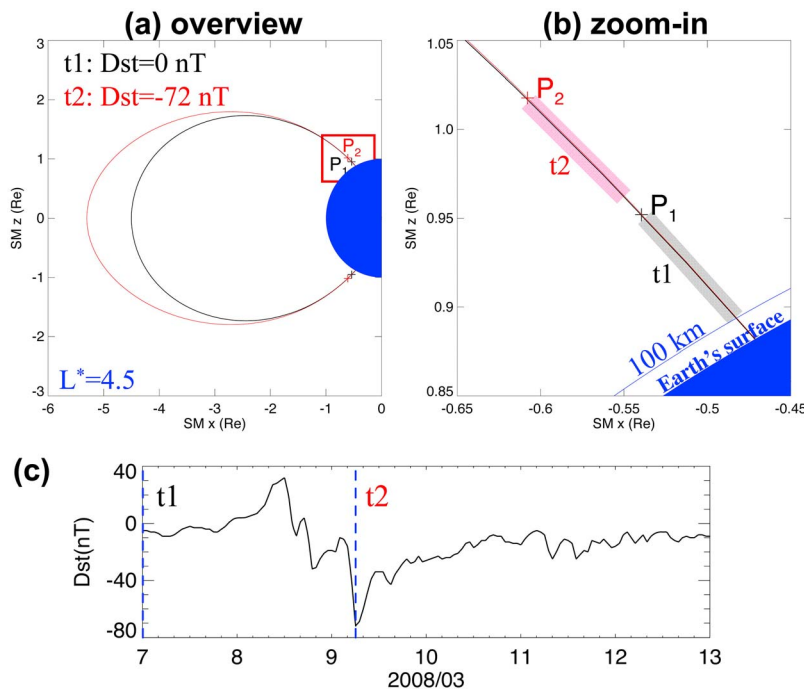
Figure 2. (a) The expansion of the drift shell and the rise of the mirror point for $L^* = 4.5$ during the storm main phase. (b) The rise of the mirror point from P_1 to P_2 (boxed region in Figure 2a). The two shaded regions represent the same electron population at two times, t1 and t2, as marked in (c) the *Dst* profile (t1 overlaps the vertical axis on left).

model, which will be introduced in section 3. Third, the rise of the mirror point implies a reduction of the magnetic field at the mirror point and thus a reduction in the electron energy due to the conservation of μ, which changes the measured electron flux for a given energy. The electrons mirroring at low altitudes have small equatorial pitch angles (for example, for *Dst* = 0 nT and $L^* = 4.5$, electrons mirroring at 600 km have an equatorial pitch angle of ~ 5.1°).

[7] Among the three adiabatic effects described above, the rise of the mirror point in altitude is unique for low-altitude observations. In Figure 2a, the rise of the mirror point appears small since it is on the scale of the entire field line. For greater detail we zoom into the boxed region of Figure 2a in Figure 2b, where the rise of the mirror point from P_1 to P_2 is more evident. The blue boundary is the Earth's surface and the blue curve, 100 km above the Earth's surface, is defined as the bounce loss cone boundary, below which energetic electrons are considered lost into the atmosphere [*Kennel*, 1969; *Blake et al.*, 2001]. As shown in Figure 2b, if all the electrons originally mirroring below P_1 (the gray region) during quiet time, t1, mirror above P_1 (the red region) at storm time, t2, a satellite at the same altitude with P_1 would see zero flux at t2. This case represents a very significant adiabatic flux change at low altitudes. We quantitatively evaluate the rise of the mirror point for a real storm in section 3.

3. Quantification of the Rise of the Mirror Point in Altitude

[8] Here we calculate the rise in altitude of the mirror point during the March 2008 storm shown in Figure 1. The problem is: given a mirror point P_1 at 600 km and $L^* = 4.5$ before the

storm (t1 in Figure 2c), find a new mirror point P_2 at the minimum *Dst* (t2 in Figure 2c), conserving all three adiabatic invariants. For the L^* and K calculation, a global magnetic field model is needed.

[9] For the analysis in this section and the following sections we chose the modified dipole model introduced by *Selesnick and Kanekal* [2009]. It combines the Earth's dipole field with a uniform southward magnetic field whose magnitude equals the *Dst* index. Figure 3 compares the pure dipole model (solid curves) with the modified dipole model (dashed curves). The dashed field lines for *Dst* = −72 nT are stretched, representing the effects of the ring current. Using this model, L^* can be calculated because it is an analytic function of r_{eq} (radial distance at the equator) and *Dst* [*Selesnick and Kanekal*, 2009, equation 10].

[10] Based on the modified dipole model, we find that in order to conserve L^* and K, electrons originally mirroring at 600 km at $L^* = 4.5$ (P_1 at time t1) mirror at 1181 km at *Dst* minimum (P_2 at t2) and, additionally, that the quiet time 100 km mirror point rises to 637 km. Therefore, all the electrons initially mirroring between 100 km and 600 km rise to between 637 km and 1181 km, indicating that a satellite at the same altitude as P_1 (600 km, ~ SAMPEX's altitude) would see no flux during the March 2008 storm at *Dst* minimum, if only considering adiabatic processes.

4. Adiabatic Changes of Electron Flux at Low Altitude

4.1. Problem and Method

[11] The three adiabatic effects work together to change the electron flux at low altitudes. Here for the March 2008 storm,
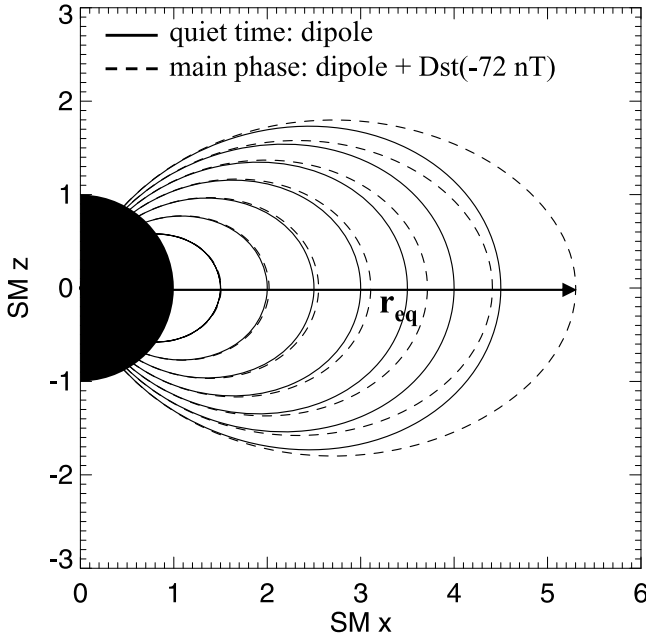
Figure 3. Comparison between the field lines of the dipole model (solid curves) and those of the modified dipole model with $Dst = -72$ nT (dashed curves).

we calculate the adiabatic flux variations of electrons mirroring at a fixed altitude and L^* (600 km, ~ SAMPEX's altitude, and $L^* = 4.5$), so that the results can be compared with observations from SAMPEX shown in Figure 1b. $L^* = 4.5$ is chosen because it is the peak flux location during this storm (Figure 1a). We look at electrons with a fixed energy. We estimate flux j_2 at 600 km and $L^* = 4.5$ for electrons with energy $E_2 = 1$ MeV at different times during the storm (total 144 points with 1 h resolution), as indicated on the top of Figure 4a. Note throughout this section, terms with subscript "1" indicate they are at fixed quiet time t1 (marked in Figure 2c); while terms with subscript "2" corresponds to time t2, times within the storm starting from t1.

[12] The calculation method for j_2 at time t2 is described as follows, corresponding to each step of the calculation procedure shown in Figure 4a:

[13] 1. Find r_{eq2}: To conserve $L^* = 4.5$, r_{eq1}, the radial distance of the field line at the equator at quiet time t1 (dipole field), is 4.5 Re (marked in Figure 4b). At time t2, given the Dst value, r_{eq2} can be calculated [*Selesnick and Kanekal*, 2009, equation 10].

[14] 2. Calculate quantities at t2: We trace the field line from the equatorial point at r_{eq2} to obtain the entire field line at $L^* = 4.5$ at t2 (the red curve in Figure 4b). Since we look at a fixed mirror point at 600 km at t2, on the red field line we can find the location of P_2, and calculate the equatorial pitch angle of electrons mirroring at P_2 as α_{eq2}, the local magnetic field strength at P_2 as B_{m2}, and the corresponding K value (2nd adiabatic invariant).

[15] 3. Calculate mapped quantities at quiet time t1: Now we have α_{eq2} and E_2 (fixed as 1 MeV), we cannot directly calculate j_2 because the energy spectrum and pitch angle distribution of j_2 varies with time. Therefore, we need to consistently map the j_2 state back to the quiet time state,

whose flux distribution is used as a fixed reference and is assumed to be

$$j_1(E, \alpha) = \begin{cases} j0 \times E^{-3} \times \sin^2 \alpha & \text{mirror point above 100 km} \\ 0 & \text{mirror point below 100 km} \end{cases}$$

$$(1)$$

The electron energy spectrum normally follows a power law with index = 3 [*Burin des Roziers and Li*, 2006] and the pitch angle distribution is assumed 90 degree peaked with power index = 2 on a sine function [*Gannon et al.*, 2007]. We used $j0 = 6.5 \times 10^5$ (#/cm^2 sr s MeV) (E in equation (1) is normalized by 1 MeV) to make the j_1 distribution consistent with the observed quiet time spectrum from the SAMPEX PET/PHA data [*Tu et al.*, 2010]. On the other hand, when the electrons are within the bounce loss cone the flux is zero. In the mapping, to conserve the K value obtained in step 2, we find the mapped, quiet time mirror point (P_1 in Figure 4b),
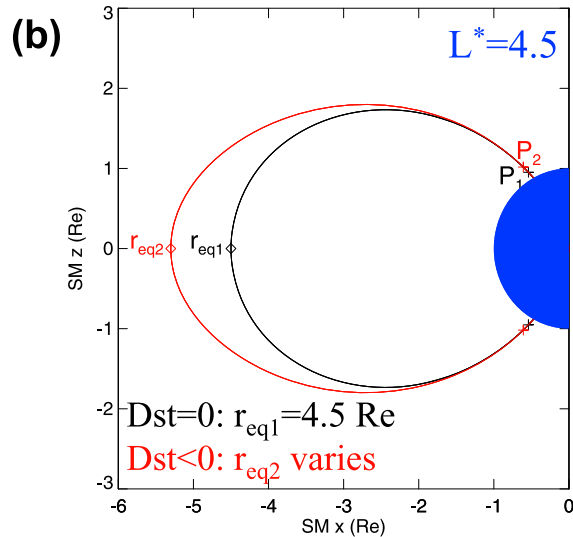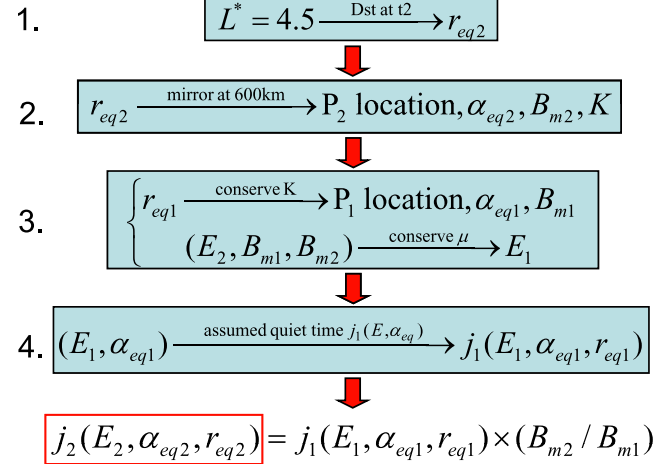

Figure 4. (a) The calculation procedure for the adiabatic flux change at a single time step during the storm, including four steps, with (b) auxiliary figure illustrations.
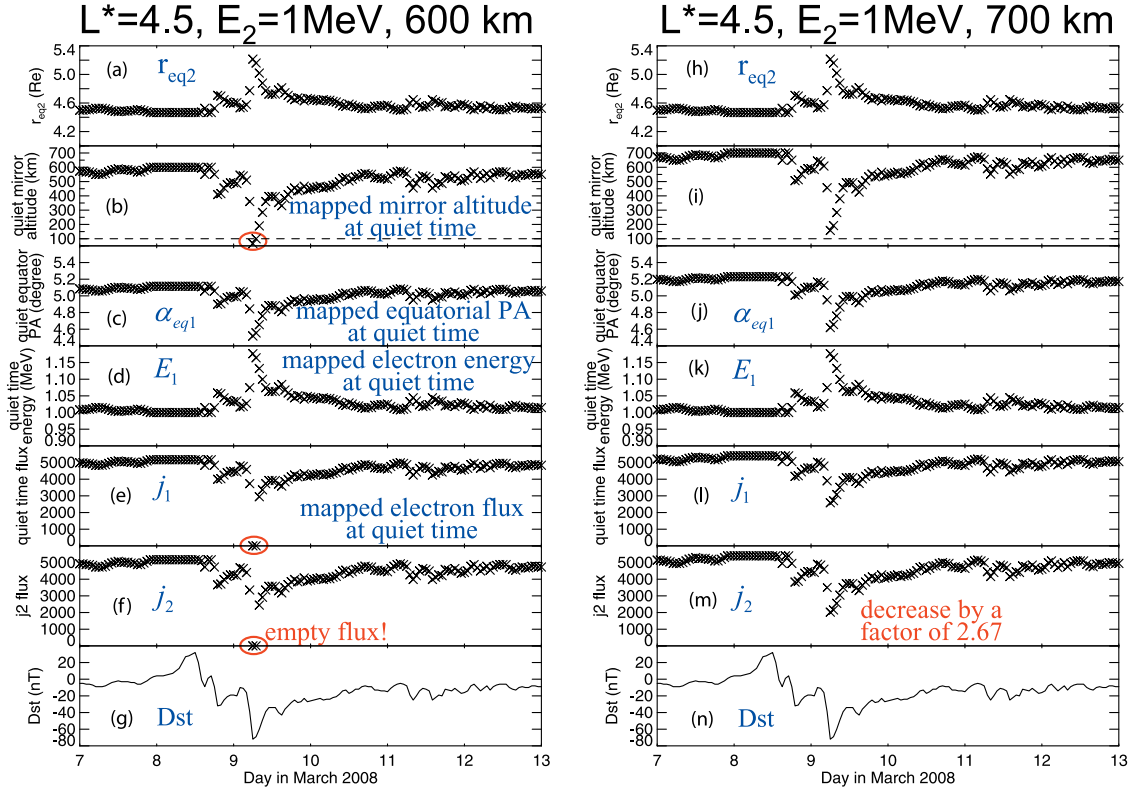
Figure 5. Calculation results for the adiabatic flux variations (j_2) at low altitude ((left) 600 km and (right) 700 km) and $L^* = 4.5$ for electrons with energy $E_2 = 1$ MeV over the entire 2008/03 storm. Figures 5a–5f and 5h–5m give intermediate results for the j_2 calculation, showing (a, h) r_{eq2}, (b, i) the mapped quiet time P_1 altitude, (c, j) α_{eq1}, (d, k) energy E_1, and (e, l) j_1, respectively. (f, m) The resulting j_2 (in units of (#/cm^2 sr s MeV)) variations. (g, n) The *Dst* profile in Figures 5g and 5n.

and acquire the magnetic field at P_1 (B_{m1}) and the equatorial pitch angle of electrons mirroring at P_1 (α_{eq1}). To find point P_1, we trace the field line from the equatorial point at r_{eq1} and iterate the calculation of K until it is equal to the K value of P_2 from step 2. Using conservation of μ, the mapped quiet time electron energy, E_1, can be calculated:

$$E_1 = -mc^2 + \sqrt{(mc^2)^2 + \frac{B_{m1}}{B_{m2}}(E_2^2 + 2mc^2 E_2)} \qquad (2)$$

[16] 4. Calculate fluxes: Using E_1, α_{eq1}, and equation (1), the mapped quiet time electron flux j_1 can be calculated. Then based on Liouville's theorem, j_2 is calculated from j_1 using the derived equation [*Schulz and Lanzerotti*, 1974; *Kim et al.*, 2010]:

$$j_2(E_2, \alpha_{eq2}, r_{eq2}) = j_1(E_1, \alpha_{eq1}, r_{eq1}) \times (B_{m2}/B_{m1}) \qquad (3)$$

4.2. Results: Two Cases of Adiabatic Flux Change at Different Altitudes

[17] We repeated the above procedure for each hour of the storm and obtained j_2 at 600 km and $L^* = 4.5$ for one MeV electrons from March 7th to March 13th. The results are shown in Figure 5 (left). Figures 5a–5g show intermediate results for calculating j_2, showing variations of r_{eq2} (from step 1 in section 4.1), altitude of the mapped mirror point P_1 at

quiet time (from step 3), mapped equatorial pitch angle α_{eq1}, energy E_1 (both from step 3), and mapped electron flux j_1 at quiet time (from step 4), respectively. The resulting j_2 variation is shown in Figure 5f, with the *Dst* profile given in Figure 5g. The variations of all the plotted quantities correlate well with the *Dst* profile. The drop of α_{eq1} and the increase of E_1 both contribute to the decrease of j_1. Near *Dst* minimum, we found two null j_1 points (circled in red), which correspond to the two points in Figure 5b (also circled) showing that the mapped mirror point at quiet time was below 100 km. Therefore, for the resulting j_2 variations, we found that the flux decreases as *Dst* drops, and disappears at minimum *Dst*.

[18] We performed the same calculation for a slightly higher altitude, 700 km. The results are shown in Figure 5 (right), in the same format as in Figure 5 (left). In this case, the altitude of the mapped mirror point at quiet time reaches a minimum of 158 km at *Dst* minimum (Figure 5i), still above the 100 km atmosphere boundary. So the flux, j_2, does not disappear, but decreases by a factor of 2.67 at *Dst* minimum (Figure 5m). This is the second case of the electron flux drop at low altitude due to the adiabatic effects during the storm main phase. These two cases are discussed further in section 5.1.

4.3. Energy Dependence of the Adiabatic Flux Change

[19] Performing the same calculation for eight logarithmically spaced energies from 0.5 to 5.66 MeV, we found that the electron flux decreases at all energies (Figure 6a). As
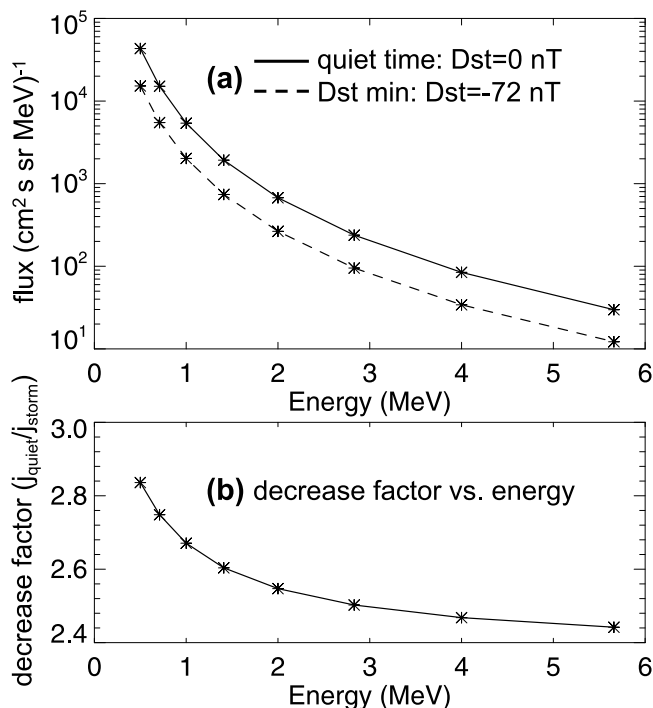
Figure 6. (a) Comparison of the energy spectrum of the quiet time electron flux at $L^* = 4.5$ and 700 km (solid line) with the calculated new energy spectrum at $Dst = -72$ nT (dashed line). (b) The decrease factors at $Dst = -72$ nT versus electron energies for electrons at $L^* = 4.5$ and 700 km altitude.

shown in Figure 6b, the decrease factors at $Dst = -72$ nT range from 2.4 to 2.8 for electrons with energies from 0.5 to 5.66 MeV at $L^* = 4.5$ and 700 km altitude. The decrease factor, which is proportional to $(E_2/E_1)^{-3}$ by equations (1) and (3), is slightly larger for lower-energy electrons, since equation (2) shows that E_1/E_2 decreases as E_2 increases, causing a lower decrease factor, or less of a decrease in flux, for higher electron energies.

5. Discussion

5.1. Altitude-Dependent Adiabatic Flux Change During Storm Time

[20] The storm-time adiabatic flux variations at a fixed low altitude were calculated to demonstrate two cases. The first case occurs when electrons originally mirroring below the investigated altitude and above the atmospheric boundary at quiet time all rise to mirror above that altitude during the storm, causing a complete dropout of the measured flux. The second case occurs when the storm-time rise of the 100 km mirror point is well below the investigated altitude, causing a fractional reduction of the flux. Separating the two cases is the maximum altitude the quiet time 100 km mirror point rises to, defined as "cutoff altitude," which is 637 km for the March 2008 storm. Thus, the magnitude of the adiabatic flux drop at low altitude is altitude-dependent. Furthermore, since the value of the "cutoff altitude" is storm-dependent (for bigger storms the mirror point rises higher because the magnetic field is further stretched), we conclude that the adiabatic flux

change at a fixed low altitude during storm time is both altitude- and storm-dependent.

[21] In the second case, the decrease factor at $Dst = -72$ nT is only 2.4–2.8 for relativistic electrons at $L^* = 4.5$ and 700 km altitude. After performing similar calculation for equatorially mirroring electrons, we found that at $Dst = -72$ nT, the flux of 1 MeV electrons mirroring at the equator decreases by a factor of 15 (as shown in Figure 7b) due to adiabatic effects, a lot more than the decrease at the low altitude in the second case. This larger decrease factor is because during storms the relative magnetic field strength decrease (B_{m2}/B_{m1}) at low altitudes is much smaller than that near equator. This results in a smaller adiabatic decrease of the electron energy from equation (2) as well as a smaller multiplication factor in equation (3), thus a smaller adiabatic flux drop at low altitudes. Even though both the energy decrease and pitch angle shift contribute to the decrease in flux of electrons mirroring at low altitudes, these effects are much smaller compared to the effect of the more significant energy decrease at the equator on the flux drop of equatorially mirroring electrons. *Kanekal et al.* [2001] found remarkable coherence of outer zone electrons by the strong correlation coefficients between electron fluxes measured at different altitudes. We also calculated the correlation coefficient between the two time series shown in Figure 7, which are both adiabatic flux variations (j_2) at $L^* = 4.5$ for $E_2 = 1$ MeV electrons over the entire 2008/03 storm, one for electrons mirroring at 700 km shown in Figure 7a, and the other for electrons mirroring at the equator in Figure 7b. The correlation coefficient is as high as 0.987, indicating the flux variations at low altitude and at the equator due to the adiabatic effects are also remarkably coherent, even though the relative decrease factors of the electron flux are quite different. The quantitative difference of the adiabatic flux variations at

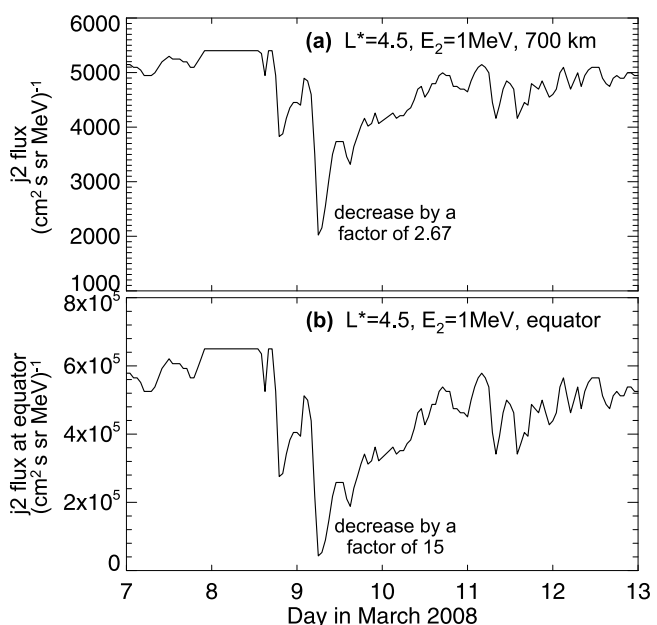**Figure 7.** Calculation results for the adiabatic flux variations (j_2) at $L^* = 4.5$ for $E_2 = 1$ MeV electrons over the entire 2008/03 storm, with results for electrons mirroring at (a) 700 km (same results as Figure 5m) and (b) the equator.
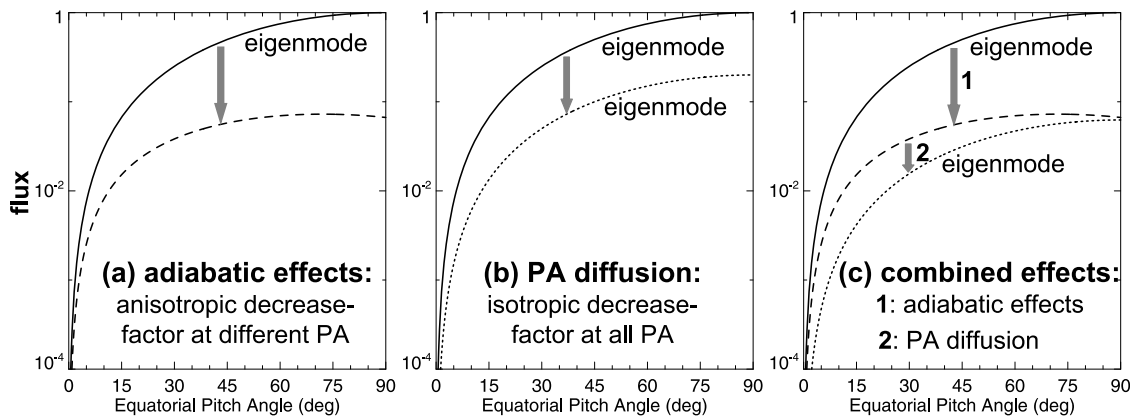
Figure 8. Diagrams showing the variations of the electron pitch angle distribution, under (a) dominant adiabatic effects, (b) dominant pitch angle diffusion, and (c) adiabatic effects plus pitch angle diffusion.

different altitudes was not so obvious until our calculations performed in this study.

5.2. Adiabatic Effects Plus Nonadiabatic Pitch Angle Diffusion

[22] The two cases above include only purely adiabatic responses. It is useful though to discuss how adiabatic and nonadiabatic processes, such as pitch angle diffusion, work together to affect the electron flux at low altitudes. In the first case previously described, electrons at 600 km disappear: in Figure 2b when all electrons move above P_1 at time t2, a null in the pitch angle distribution is created for electrons mirroring above 100 km and below 637 km (the lower end of the red region). Under moderate pitch angle diffusion, this void in the pitch angle distribution can be filled quickly. For example, at t2 the mirror point at 637 km corresponds to an equatorial pitch angle of 3.23°, while the mirror point at 100 km corresponds to an equatorial pitch angle of 2.85°; assuming a pitch angle diffusion rate D_{xx}, as defined by *Schulz and Lanzerotti* [1974], equal to 10^{-9}/s (corresponding to electron e-folding lifetime ∼ 100 days [*Tu et al.*, 2010]) filling the void in the pitch angle distribution takes only several minutes. Then the electron flux would not drop to zero but instead by a factor similar to that seen in the second case. However, since the pitch angle diffusion rate, caused by resonance with a variety of plasma waves, depends on the spectral and latitudinal distribution of the wave power, the ratio of the plasma frequency to electron gyrofrequency (f_{pe}/f_{ce}), the distribution of wave normal angles, and the electron energies etc., the D_{xx} for MeV energy electrons at low altitude can at times be much slower than 10^{-9}/s [*Li et al.*, 2007; *Horne et al.*, 2009]. For example, based on the results shown in Figure 2 of *Li et al.* [2007] we know that D_{xx} from chorus waves for 1 MeV electrons at equatorial pitch angles near 3.23° can be less than 10^{-12}/s. For $D_{xx} = 10^{-12}$/s, filling the zero fluxes at the low altitudes now takes about a day, while adiabatic processes act on time scales on the order of hours or shorter. Therefore, the null fluxes at the low altitudes created by adiabatic effects can persist for very slow pitch angle diffusion.

[23] From previous calculations and discussions, we understand that the different levels of adiabatic flux drops at different equatorial pitch angles change the electron pitch angle distribution as a magnetic storm develops, as illustrated

in Figure 8a with larger drop at the equator from the adiabatic effects than at low altitudes. Simultaneously, nonadiabatic pitch angle diffusion also evolves the pitch angle distribution from an arbitrary initial distribution to an equilibrium state, which is the lowest-order eigenmode of the bounce-averaged pitch angle diffusion operator [*Shprits et al.*, 2006; *Albert and Shprits*, 2009]. The equilibrium state decays steadily in time with the decay rate represented by the corresponding eigenvalue of the lowest-order eigenmode that is independent of the electron pitch angle. Higher-order eigenmodes may be included in the initial phase of the evolution, but they decay much faster [*Selesnick et al.*, 2003]. Note all the initial pitch angle distributions in Figures 8a–8c are assumed as the equilibrium eigenmode-shape reached after sustained pitch angle diffusion. Therefore, after reaching the equilibrium eigenmode, pitch angle diffusion keeps an isotropic decrease factor for all the electron pitch angles, as shown in Figure 8b.

[24] Adiabatic processes and pitch angle diffusion may occur simultaneously, but at different time scales. As illustrated in Figure 8c, after reaching the equilibrium eigenmode by pitch angle diffusion, adiabatic effects bring the distribution to the dashed curve (step 1 in Figure 8c), same as in Figure 8a with different decrease factors at different pitch angles. The dashed curve then serves as an initial distribution for the pitch angle diffusion. Therefore, if the pitch angle diffusion rate remains roughly constant throughout the storm, pitch angle diffusion tends to restore the pitch angle distribution to the same eigenmode shape (step 2 in Figure 8c). The time required to relax the initial distribution (the dashed curve) to the equilibrium eigenmode (the dotted curve), named the "relaxation time," depends on the strength of the pitch angle diffusion rate and how far the initial distribution is from the lowest-order eigenmode. For the case where the relaxation time scale is on the same order as the adiabatic change time scale or shorter, pitch angle diffusion can isotropize the relative flux reduction at the equator and at low altitudes (illustrated by step 1 plus step 2 in Figure 8c or by Figure 8b with pitch angle diffusion dominant than the adiabatic effects). Furthermore, since the adiabatic effects continuously reshape the pitch angle distribution away from the lowest-order eigenmode, during the pitch angle diffusion, higher-order eigenmodes will be consistently excited, which decay faster in time and will cause increased electron precipitation without changing the pitch angle diffusion rate. To

quantify the additional precipitation from the adiabatic change in the electron pitch angle distribution requires detailed modeling, which will be conducted in the future work. On the other hand, if the relaxation time scale is much slower than the adiabatic change time scale, which is possible during weak pitch angle diffusion, the anisotropic adiabatic flux changes at different pitch angles will remain during the storm time and the pitch angle distribution will barely return to the eigenmode (close to the case in Figure 8a with adiabatic effects dominant than pitch angle diffusion).

5.3. Comparison With SAMPEX Data

[25] It is useful to compare the adiabatic flux drops from the two cases to observed data to answer the two questions raised at the end of section 1, or equivalently, to what degree adiabatic changes can account for flux variations observed by SAMPEX during storms. Notice that our calculation results are for electrons locally mirroring at 600 and 700 km, while SAMPEX is actually in a ~550 × 675 km orbit with a wide detector opening angle [*Cook et al.*, 1993]. Thus the integral flux measured by SAMPEX is a weighted average of electrons mirroring at and below SAMPEX (a range of mirror point altitudes), able to cover electrons in either of these two cases discussed previously or both of them. For example, if all the electrons detected by SAMPEX mirror at altitudes belonging to the second case, SAMPEX would see a fractional flux drop; in contrast, if the electrons detected by SAMPEX partly or entirely fall into the "null flux" case, the measured integral flux would drop more. Realistic simulation of the adiabatic integral flux change detected by SAMPEX requires integration over a range of pitch angles and energies covered by the detector based on its angular and energy responses, as well as implementing SAMPEX's orbit in a realistic magnetic field model, which is much more complicated than the calculations performed in section 4 for locally mirroring electrons.

[26] The SAMPEX data in Figure 1b indicates that the trapped electron count rates (green points) at L = 4.5 decreased by almost an order of magnitude during the storm main phase. This demonstrates that the second case is not the main form of adiabatic effects during this storm, since it can only account for a small fraction of the observed flux drop. Then is it nonadiabatic processes that play a leading role in the storm-time flux drop? Or is it due to some other forms of adiabatic flux change at SAMPEX, e.g., a weighted combination of the first and the second cases as discussed above? Adiabatic effects have little influence on the flux of the drift loss cone electrons, since they will be lost within one electron drift period, which is much faster than the adiabatic changes. Data shows that during the storm main phase the trapped electrons decrease more significantly than the drift loss cone electrons (blue points), meanwhile the drift loss cone electrons exhibit a flatter distribution over longitude compared with the prestorm interval. These are all indicators of enhanced pitch angle diffusion [*Tu et al.*, 2010]. Therefore, even though we cannot answer exactly how much of the observed trapped electron flux drop during the storm main phase is from the adiabatic effects due to the difficulties described above, we can still conclude that the observed storm-time flux variations at SAMPEX are not purely adiabatic responses, and nonadiabatic processes are dominant in this event.

[27] In section 4 we analyzed the adiabatic flux change for electrons mirroring at a fixed altitude (~ SAMPEX's altitude) and fixed $L^* = 4.5$, rather than at a fixed point in space. This differs from the analysis performed by *Kim and Chan* [1997] for a fixed point at geosynchronous altitude, which is at different L^* for different times within the storm due to the adiabatic expansion of the drift shell. For example, for a fixed equatorial point at r_{eq1} in Figure 4b (4.5 Re), its L^* changes from 4.5 at quiet time to $L^* = 4.06$ at $Dst = -72$ nT calculated using the modified dipole model. Therefore, since the fixed point maps to different L^* shells at quiet times, to estimate the storm-time adiabatic effects for a fixed point at the equator requires further consideration of the radial dependence of the quiet time electron flux in addition to the energy and pitch angle dependences [*Kim and Chan*, 1997]. However, for a fixed point at low altitude, the change of L^* during a storm is much less than that at equator, due to the fact that most of the drift shell expansion occurs at high altitude (or lower latitude), as seen in Figure 2a, where the black and red field lines almost colocate at P_1 altitude (more evident in Figure 2b). More quantitatively the L^* of a fixed point at P_1 at 600 km initially with $L^* = 4.5$ at quiet time, decreases to 4.49 at $Dst = -72$ nT, almost negligible compared to the L^* change at the equator. Taking this into account, our conclusions from looking at electrons mirroring at a fixed altitude and fixed L^* are expected to be similar to those at a fixed point in space at low altitude.

5.4. Uncertainties in the Quantitative Results

[28] As a final point, we discuss the possible uncertainties of our quantitative results. First, for the quiet time flux distribution in equation (1), we chose 3 as the power law index for the energy dependence and 2 as the power index for the sine-form pitch angle dependence. The choice of these two numbers affects the calculated decrease factors in section 4.2. For example, the pitch angle distribution $\sin^2 \alpha$ is obtained from *Gannon et al.* [2007] by fitting to quiet time CRRES data near the equator, which is actually not capable of resolving the pitch angle distribution at low altitudes near the loss cone that is relevant to our study. Thus, the lack of a clear picture of the pitch angle distribution near the loss cone could introduce uncertainties to our calculation results. Specifically, the results show that when the power index for the pitch angle dependence changes from 2 to 5, the range of the decrease factors shown in Figure 6b changes from 2.4–2.8 to 3.5–4.1, but the qualitative conclusions in the paper remain unaffected. Similarly, moving the atmospheric boundary from 100 km to a different altitude, e.g., 80 km or 120 km, would change the value of the "cutoff altitude," but again the overall conclusions remain valid.

[29] The quantitative results for these adiabatic flux decrease factors and the value of the "cutoff altitude" depend on the magnetic field model used in the calculation. In this work we used the modified dipole model due to its simplicity. It is useful to compare the results from the simplified model with a more realistic model. A similar calculation on the rise of the mirror point in altitude as in section 3 was performed using the Tsyganenko 2001 storm-time field model (T01S) [*Tsyganenko*, 2002a, 2002b]. We looked at electron mirror points in the midnight plane, southern hemisphere, and found that the 600 km mirror point rises to 1356 km at *Dst* minimum,

and the 100 km mirror point rises to 851 km, implying a null flux at 600 km at *Dst* minimum. The calculated rise of the mirror point in altitude using the T01S model is larger than that using the modified dipole model by ~200 km. This can be understood by looking at the solar wind dynamic pressure data during the storm main phase (not shown here), which remains high and further stretches the magnetic field on the nightside. This effect is not included in the simplified field model, which primarily captures the global ring current effects. However, the modified dipole model still provides reasonable results, generally comparable to those using T01S model.

5.5. Future Applications

[30] As discussed before, the variations in observed data are due to a combination of both adiabatic and nonadiabatic effects and to simulate the observed electron variations a physical model must include both adiabatic and nonadiabatic processes. However, currently most models simulating electron losses do not include adiabatic losses. For example, the *Tu et al.* [2010] model represents the low-altitude electron distribution as a balance of pitch angle diffusion, azimuthal drift and possible sources, and is used to quantify the electron lifetimes from the estimated loss rate D_{xx} by fitting the model results to SAMPEX data. However, adiabatic losses are not explicitly included in the model, which can be improved by applying the adiabatic analysis performed here. Specifically, we can include the adiabatic corrections at each simulation time step, updating the modeled phase space densities as a function of energy and equatorial pitch angle with the adiabatically corrected ones. By including adiabatic corrections, the model fit to the data can be improved and the pitch angle diffusion rate can be more accurately determined.

6. Conclusions

[31] The work presented is the first quantitative study of the storm-time adiabatic effects on radiation belt electrons at low altitudes. The adiabatic effects on low-altitude electrons during the storm main phase include the expansion of the drift shell, the rise of electron mirror point in altitude and the shift in the energy spectrum of the electron flux. We find that even for the moderate storm of March 2008, the rise of the mirror point is sufficient to cause a complete disappearance of the electron flux at SAMPEX's altitude.

[32] Calculations of adiabatic flux changes at a fixed low altitude suggest two cases, well-separated by a "cutoff altitude" defined as the highest altitude the mirror point, originally located at 100 km (the sharp atmospheric bounce loss cone boundary) during quiet time, rises to for a given storm. Due to adiabatic effects, a satellite below the "cutoff altitude" sees no flux for some time during the storm main phase, because electrons originally mirroring below the satellite and above the atmospheric boundary at quiet times now all move to mirror above the satellite. The second case is for a satellite at low altitude located well above the "cutoff altitude," which sees a fractional flux drop of locally mirroring electrons during the storm. The drop is less than that seen in equatorially mirroring electrons. These two cases suggest that the adiabatic flux change at a fixed low altitude during storms is both altitude- and storm-dependent, and it is not simply analogous to that for equatorially mirroring electrons.

[33] However, generally the flux variations at low altitudes depend on the relative time scales of adiabatic processes and nonadiabatic processes, such as pitch angle diffusion. Even though moderate pitch angle diffusion can quickly fill the "null flux" case, under certain circumstances the pitch angle diffusion for relativistic electrons can be very slow during storms and the zero flux at the low altitudes created by adiabatic effects can persist. Pitch angle diffusion also tends to relax the pitch angle distribution to the lowest-order eigenmode of the bounce-averaged pitch angle diffusion operator. If the relaxation time scale is shorter or on the same order of the adiabatic processes, pitch angle diffusion would isotropize the relative flux reduction at the equator and at low altitudes. Furthermore, the adiabatic change in the electron pitch angle distribution can result in increased electron precipitation by exciting higher-order eigenmodes of pitch angle diffusion without changing the pitch angle diffusion rate. By comparing the calculated adiabatic flux change with data for the March 2008 storm and by further investigating the variations of the drift loss cone electron flux, we found that even though adiabatic processes contribute to the decrease of the trapped electron flux observed in the main phase, nonadiabatic processes are still dominant for this particular event. For future applications the adiabatic analysis performed here can be used to improve loss models of outer radiation belt electrons [e.g., *Tu et al.*, 2010].

References

Albert, J. M., and Y. Y. Shprits (2009), Estimates of lifetimes against pitch angle diffusion, *J. Atmos. Sol. Terr. Phys.*, *71*, 1647–1652, doi:10.1016/j.jastp.2008.07.004.

Baker, D. N., and S. Kanekal (2008), Solar cycle changes, geomagnetic variations, and energetic particle properties in the inner magnetosphere, *J. Atmos. Sol. Terr. Phys.*, *70*(2–4), 195–206, doi:10.1016/j.jastp.2007.08.031.

Baker, D. N., et al. (1993), An overview of the SAMPEX mission, *IEEE Trans. Geosci. Remote Sens.*, *31*, 531–541, doi:10.1109/36.225519.

Blake, J., et al. (2001), Lightning-induced energetic electron flux enhancements in the drift loss cone, *J. Geophys. Res.*, *106*(A12), 29,733–29,744, doi:10.1029/2001JA000067.

Burin des Roziers, E., and X. Li (2006), Specification of >2 MeV geosynchronous electrons based on solar wind measurements, *Space Weather*, *4*, S06007, doi:10.1029/2005SW000177.

Cook, W. R., et al. (1993), PET: A proton/electron telescope for studies of magnetospheric, solar, and galactic particles, *IEEE Trans. Geosci. Remote Sens.*, *31*, 565–571, doi:10.1109/36.225523.

Friedel, R. H. W., G. Reeves, and T. Obara (2002), Relativistic electron dynamics in the inner magnetosphere: A review, *J. Atmos. Sol. Terr. Phys.*, *64*, 265–282, doi:10.1016/S1364-6826(01)00088-8.

Gannon, J. L., X. Li, and D. Heynderickx (2007), Pitch angle distribution analysis of radiation belt electrons based on Combined Release and Radiation Effects Satellite Medium Electrons A data, *J. Geophys. Res.*, *112*, A05212, doi:10.1029/2005JA011565.

Horne, R. B., M. M. Lam, and J. C. Green (2009), Energetic electron precipitation from the outer radiation belt during geomagnetic storms, *Geophys. Res. Lett.*, *36*, L19104, doi:10.1029/2009GL040236.

Kanekal, S., D. Baker, and J. Blake (2001), Multisatellite measurements of relativistic electrons: Global coherence, *J. Geophys. Res.*, *106*(A12), 29,721–29,732, doi:10.1029/2001JA000070.

Kennel, C. F. (1969), Consequences of a magnetospheric plasma, *Rev. Geophys.*, *7*(1, 2), 379–419, doi:10.1029/RG007i001p00379.

Kim, H.-J., and A. A. Chan (1997), Fully adiabatic changes in storm time relativistic electron fluxes, *J. Geophys. Res.*, *102*, 22,107–22,116, doi:10.1029/97JA01814.

Kim, K. C., et al. (2010), Numerical estimates of drift loss and *Dst* effect for outer radiation belt relativistic electrons with arbitrary pitch angle, *J. Geophys. Res.*, *115*, A03208, doi:10.1029/2009JA014523.

Li, W., Y. Y. Shprits, and R. M. Thorne (2007), Dynamic evolution of energetic outer zone electrons due to wave-particle interactions during storms, *J. Geophys. Res.*, *112*, A10220, doi:10.1029/2007JA012368.

Li, X., and M. A. Temerin (2001), The electron radiation belt, *Space Sci. Rev.*, *95*, 569, doi:10.1023/A:1005221108016.

Li, X., et al. (1997), Multisatellite observations of the outer zone electron variation during the November 3–4, 1993, magnetic storm, *J. Geophys. Res.*, *102*(A7), 14,123–14,140, doi:10.1029/97JA01101.

McIlwain, C. E. (1966), Ring current effects on trapped particles, *J. Geophys. Res.*, *71*, 3623–3628.

McIlwain, C. E. (1996), Processes acting upon outer zone electrons, in *Radiation Belts: Models and Standards*, *Geophys. Monogr. Ser.*, vol. 97, edited by J. F. Lemaire, D. Heynderickx, and D. N. Baker, pp. 15–26, AGU, Washington, D. C.

Millan, R. M., and R. M. Thorne (2007), Review of radiation belt relativistic electron loss, *J. Atmos. Sol. Terr. Phys.*, *69*, 362–377, doi:10.1016/j.jastp.2006.06.019.

Reeves, G. D., et al. (2003), Acceleration and loss of relativistic electrons during geomagnetic storms, *Geophys. Res. Lett.*, *30*(10), 1529, doi:10.1029/2002GL016513.

Roederer, J. G. (1970), *Physics and Chemistry in Space*, vol. 2, *Dynamics of Geomagnetically Trapped Radiation*, 166 pp., Springer, Berlin.

Schulz, M., and L. Lanzerotti (1974), *Particle Diffusion in the Radiation Belts*, Springer, New York.

Selesnick, R. S. (2006), Source and loss rates of radiation belt relativistic electrons during magnetic storms, *J. Geophys. Res.*, *111*, A04210, doi:10.1029/2005JA011473.

Selesnick, R. S., and S. G. Kanekal (2009), Variability of the total radiation belt electron content, *J. Geophys. Res.*, *114*, A02203, doi:10.1029/2008JA013432.

Selesnick, R. S., J. B. Blake, and R. A. Mewaldt (2003), Atmospheric losses of radiation belt electrons, *J. Geophys. Res.*, *108*(A12), 1468, doi:10.1029/2003JA010160.

Shprits, Y. Y., W. Li, and R. M. Thorne (2006), Controlling effect of the pitch angle scattering rates near the edge of the loss cone on electron lifetimes, *J. Geophys. Res.*, *111*, A12206, doi:10.1029/2006JA011758.

Tsyganenko, N. A. (2002a), A model of the near magnetosphere with a dawn-dusk asymmetry: 1. Mathematical structure, *J. Geophys. Res.*, *107*(A8), 1179, doi:10.1029/2001JA000219.

Tsyganenko, N. A. (2002b), A model of the near magnetosphere with a dawn-dusk asymmetry: 2. Parameterization and fitting to observations, *J. Geophys. Res.*, *107*(A8), 1176, doi:10.1029/2001JA000220.

Tu, W., X. Li, Y. Chen, G. D. Reeves, and M. Temerin (2009), Storm-dependent radiation belt electron dynamics, *J. Geophys. Res.*, *114*, A02217, doi:10.1029/2008JA013480.

Tu, W., R. Selesnick, X. Li, and M. Looper (2010), Quantification of the precipitation loss of radiation belt electrons observed by SAMPEX, *J. Geophys. Res.*, *115*, A07210, doi:10.1029/2009JA014949.

X. Li and W. Tu, LASP, University of Colorado at Boulder, 1234 Innovation Dr., Boulder, CO 80303, USA. (tu@colorado.edu)